P.221 Impact of Assimilating CASA X-Band Radar Data for 24 May 2011 Tornadic Storms Using Various Microphysics Schemes at 1-km Grid Spacing

Derek R. Stratman[1,2] * and Keith A. Brewster[1]
[1]Center for Analysis and Prediction of Storms, Norman, Oklahoma
[2]School of Meteorology, University of Oklahoma, Norman, Oklahoma

1. INTRODUCTION

On the afternoon of 24 May 2011, an outbreak of twelve tornadoes, including two EF-4 tornadoes and one EF-5 tornado, invaded northern and central Oklahoma within the Norman, OK, National Weather Service (NWS) Weather Forecast Office's county warning area. This outbreak caused 11 deaths and 293 injuries (see http://www.srh.noaa.gov/oun/?n=events-20110524 for more information). An extensive observation network was in place in this area during the spring of 2011, so despite the tragic loss of life, this is an ideal case to explore aspects of the Warn-on-Forecast (WoF) concept (Stensrud et al., 2009, 2013) with storm-scale numerical simulations.

The tight clustering of the tornadic and non-tornadic supercells on this date made forecasting of storm tracks difficult for storm-scale models, but the Center for Analysis and Prediction of Storms (CAPS) real-time forecasting system had good success at simulating these storms. The impact of assimilating CASA X-band radar data on the ability of forecasts to simulate the storms and their structure, and how this varies with different microphysics schemes, has not previously been examined for this case. Therefore, this study's aim is to examine the effect of assimilating CASA radar data using five different microphysics parameterization schemes (Table 1) on the tracks of simulated mesocyclones (MC) via the updraft helicity (UH) field as compared to each other and reality (i.e., estimated tornado point locations) in a potential future WoF framework.

Instead of using vertical vorticity to identify and track MC centers (as in, e.g., Trapp and Weisman, 2003 and Schenkman et al., 2011), updraft helicity (UH; Kain et al., 2008, which used UH from 2 to 5 km AGL) is used because UH is the integral of the product of vertical vorticity and vertical velocity through a designated depth. The UH centers are compared to each other and reality via observed tornado point locations. Similar to hurricane center errors (e.g., Xue et al., 2013), UH center distance and timing errors are computed to assess model performance.

Recently, the Advanced Regional Prediction System's (ARPS; Xue et al., 2000; Xue et al., 2001; Xue et al., 2003) data assimilation system's (ADAS) complex cloud analysis package (Hu et al., 2006a,b) was updated for several microphysics schemes, including the five in this study (Brewster and Stratman, 2015). The goal of this update was to improve analyses of hydrometeors using scheme-specific reflectivity inversion equations.

The numerical simulation methodology for this study, including details about the observational data and model settings, are described in section 2. The verification methodology is described in section 3. Results from the first experiment are presented in section 4, and preliminary results from the second experiment are presented in section 5. Lastly, section 6 will provide a summary and discussion of the results, along with potential future work.

2. SIMULATION METHODOLOGY

Since this experiment intends to explore the capabilities of the forecast system in a realistic qausi-operational setting, the numerical simulations use data from multiple observing platforms. Surface observations from NWS and FAA METAR and Oklahoma Mesonet stations along with radial wind and reflectivity data from the WSR-88D [Dallas/Fort Worth (KFWS), Dodge City (KDDC), Frederick (KFDR), Tulsa (KINX), Twin Lakes (KTLX), Vance (KVNX), and Wichita (KICT)] and Collaborative Adaptive Sensing of the Atmosphere (CASA) IP-1 [Chickasha (KSAO), Cyril (KCYR), Lawton (KLWE), and Rush Springs (KRSP); see Fig. 1] radar networks (McLaughlin et al., 2009) are ingested into the initial analyses of the numerical simulations.

The 1800 UTC 12-km NAM (North American Mesoscale) model's 3-hour forecast is used as a background field in CAPS' ARPS's three-dimensional variational (3DVAR; Gao et al., 2004) and complex cloud analysis process to produce an initial analysis on a 323x353-km domain with 1-km horizontal grid spacing (Fig. 1) and 53 vertically-stretched levels with a minimum vertical grid spacing of 20 m at the bottom. Three analysis passes with 20, 50, and 50 iterations and horizontal influence radii of 45, 2, and 1 km, respectively, are used to produce the 3DVAR analysis through the minimization of the cost function. The surface in-situ data is implemented in the first and third passes, while the radar data is applied in the second and third passes. In addition, a 3D mass divergence

* *Corresponding author address:* Derek R. Stratman, The Univ. of Oklahoma, School of Meteorology, Norman, OK 73072; e-mail: stratman@ou.edu

constraint is utilized to couple the wind components together (Hu et al., 2006b). The cloud analysis uses cloud observations from surface and satellite and hydrometeor data from radar after the mass field is obtained via 3DVAR.

An ARPS model simulation is integrated to produce forecasts out to 125 minutes. During the first 5 min, an incremental analysis update (IAU, Bloom et al., 1996) assimilation is performed by introducing the analysis increments every 20 s. The increments are applied to all fields except for vertical velocity and pressure since those two fields are not directly observed in 3D and will quickly respond to the other fields to create a balanced state. The simulation proceeds on its own for the remaining 120 min.

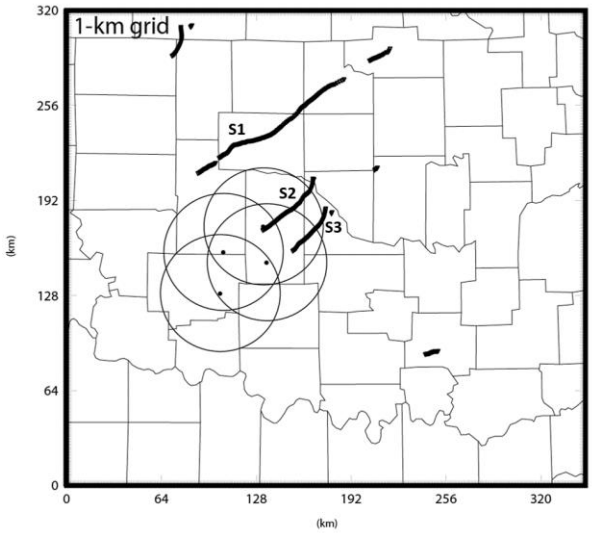

Figure 1. Domain of numerical simulations with CASA radar locations and 40-km range rings, estimated tornado points, and storm IDs.

During the integration of ARPS, a big and small time step of 2.0 s and 0.5 s, respectively, are employed in the leapfrog time formulation. In addition, the 1800 UTC 12-km NAM forecasts are used for the lateral boundary conditions. Some other model details include: 4th-order momentum advection in both the horizontal and vertical directions, scalar advection using Zalesak's multi-dimensional version of flux-corrected transport (Zalesak, 1979), 1.5-order TKE closure based on Sun and Chang (1986), 4th-order computational mixing, Rayleigh damping beginning at 12-km AGL, National Aeronautics and Space Administration atmospheric radiation transfer parameterization, surface fluxes calculated from stability-dependent surface drag coefficients using predicted surface temperature and volumetric water content, and two-layer force-store soil model based on Noilhan and Planton (1989). The modeling process is summarized with a flow chart in Figure 2.

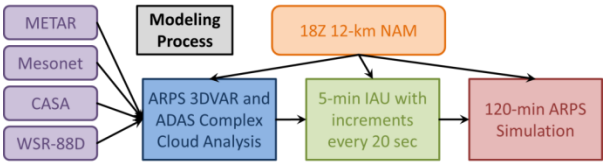

Figure 2. Flow chart of the modeling process used in this numerical simulation experiment.

Research experiments are done using five different microphysics parameterization schemes: Lin 3-ice microphysics scheme (Lin et al., 1983), Weather Research and Forecasting (WRF) single-moment 6-class microphysics scheme (Hong and Lim, 2006), Milbrandt and Yau (MY) single-moment bulk microphysics scheme, MY double-moment bulk microphysics scheme, and MY triple-moment bulk microphysics scheme (Milbrandt and Yau 2005a,b; Table 1).

ID	Microphysics Scheme
LIN3	Lin 3-ice microphysics
WSM6	Weather Research and Forecasting single-moment 6-class microphysics
MYSM	Milbrandt and Yau (MY) single-moment bulk microphysics
MYDM	MY double-moment bulk microphysics
MYTM	MY triple-moment bulk microphysics

Table 1. List of microphysics schemes used in the numerical simulations with their associated ID names.

In addition to microphysics diversity, simulations are run using a potential future WoF framework. Eight simulations are integrated every 30 minutes starting at 1900 UTC (IAU begins at 1855 UTC) and ending at 2230 UTC (Table 2). With this WoF framework, the time of tornado genesis (dissipation) for each of the storms of interest is captured by four (at least one) simulations. The first storm (S1; storms depicted in Fig. 1) developed and stayed outside the CASA radar network and produced two tornadoes, including the outbreak's only EF-5 tornado. The second and third storms (S2 and S3, respectively) developed in the CASA radar network and both produced EF-4 tornadoes, which dissipated before impacting the Oklahoma City metro area.

Two experiments are conducted to examine the impact of assimilating CASA radar data with the various microphysics schemes on the tracking of the MC centers. The first experiment compares assimilating all available data (Control) and assimilating all available

data except the CASA radar data (NoCASA). This experiment is performed using the entire WoF framework. The second experiment explores what would happen if KTLX would have been unavailable for the initiation of the 2130 UTC simulations. In addition to the Control and NoCASA runs from the first experiment, simulations assimilating all available data except KTLX radar data (NoKTLX) and simulations assimilating all available data excluding CASA and KTLX radar data (Neither) are executed for the simulations initialized at 2130 UTC.

ARPS Begin – End	S1 2031 Z - 2046 Z 2050 Z - 2235 Z 2250 Z - 2305 Z	S2 2206 Z - 2301 Z	S3 2226 Z - 2305 Z 2302 Z - 2303 Z
1900 Z – 2100 Z	+1:31		
1930 Z – 2130 Z	+1:01		
2000 Z – 2200 Z	+0:31		
2030 Z – 2230 Z	+0:01	+1:36	+1:56
2100 Z – 2300 Z	-0:29	+1:06	+1:26
2130 Z – 2330 Z	-0:59	+0:36	+0:56
2200 Z – 0000 Z	-1:29	+0:06	+0:26
2230 Z – 0030 Z	-1:59	-0:24	-0:04

Table 2. Storm ID names and associated tornado and ARPS-simulation forecast times. Positive (green) and negative (red) values indicate the time difference between the start of the simulations and first tornadogenesis for each of the storms.

3. VERIFICATION METHODOLOGY

To assess model performance, simulated MC centers via the UH field are compared to each other and verified using tornado locations estimated from observations. The locations of the six tornadoes associated with the three storms of interest are estimated every minute based on NWS damage surveys, radar data, and high-resolution aerial photos from Google Maps. Two adjacent layers of UH (namely, 1–6 km and 0–1 km) are used for the verification of the simulations. These two layers are intended to represent simulated mid-level and low-level mesocyclones, respectively. As mentioned before, Kain et al. (2008) used UH from 2 to 5 km AGL to signify mid-level mesocyclones, but for this study, a deeper layer of UH is utilized to give more robust UH values by capturing more of the simulated mid-level MCs.

Since UH is a 2D field and not point data, a simple 2D object-based technique is utilized to find UH-weighted centers (analogous to mass-weighted centers), which will be compared to the estimated tornado points. A search radius of 10 km (i.e., 10 grid points) is used to isolate 1–6-km (0–1-km) UH maxima that are greater than or equal to 400 $m^2 s^{-2}$ (20 $m^2 s^{-2}$) and their surrounding grid point values. A max UH value is considered a UH-center candidate if 4 out of 8 (3 out of 8) of the adjacent grid point values equals or exceeds 200 $m^2 s^{-2}$ (10 $m^2 s^{-2}$). Once the UH-center candidates are determined, the UH-weighted center is computed using a radius of 5 km extending from the grid point with the max UH value.

With the UH-weighted center locations, an objective verification technique is used to quantify location and timing errors. First, distance errors are computed between the estimated tornado point locations and the nearest UH center locations at coincident times (referred to as “same time”, or ST, for rest of paper). Second, distance and timing errors are calculated between the estimated tornado point locations and the nearest UH center locations at any time during the life of the tornadoes of interest (referred to as “any time”, or AT, for rest of paper).

Differences between averaged distance and timing errors are plotted for assessment of the first experiment. Negative values for distance error differences indicate the Control run performed better than the NoCASA run. For differences in timing errors, absolute values of the timing errors are used, so once again, negative values indicate the Control run performed better. Since the second experiment only focuses on the 2130 UTC simulations, column charts of the average distance and timing errors are used.

4. Control vs. NoCASA

4.1 *Storm 1*

Except for the 2230 UTC simulations’ 0–1-km UH (0-1UH) centers, the ST and AT average distance error differences between the Control and NoCASA runs are somewhat evenly spread within 5 km above and below the no difference line (Fig. 4a,b,d,e). The differences of the absolute values of the timing errors are generally less than 10 minutes, so this means there are timing error differences up 20 minutes between the Control and NoCASA runs (Fig. 4c,f). Also, there is no impact on this metric by assimilating CASA radar data for the 1900 UTC simulations. Interestingly, the Control runs tend to perform slightly better for the 0-1UH centers, but the opposite is generally true for the 1–6-km UH (1-6UH) centers. However, the results depict fairly small differences between the two types of simulations, so even though assimilating CASA radar has some impact on the forecasts, the benefits for S1 are not apparent. This in not unexpected because S1 was outside of the range of the CASA radars.

4.2 *Storm 2*

The spread in differences for S2 is larger than for S1, but the impact of assimilating CASA radar data is more evident with S2 than S1. In general, the Control runs have smaller ST and AT average distance errors

revealing the positive impact of assimilating CASA radar data when simulations are initialized within the CASA radar network (Fig. 5a,b,d,e). There is considerable variability among the different microphysics schemes with respect to differences in average timing errors, but overall, the Control runs tend to have smaller timing errors (Fig. 5c,f).

4.3 *Storm 3*

The simulations all tend to suffer somewhat with forecasting S3 by failing to properly evolve and sustain the original storm, so fewer UH centers meet the threshold requirements used for verification. This leads to larger spreads in average distance and timing error differences, especially for 0-1UH (Fig. 6). Because of difficulties found in forecasting for S3, the results are mixed and unreliable.

5. EFFECT of REMOVING KTLX DATA?

The KTLX radar is fairly close to the storms of interest, and Oklahoma has relatively dense WSR-88D network coverage. The KTLX data are removed in these experiments to assess the impact of gap-filling radar data, such as CASA, under conditions with more widely spread WSR-88D radars or in the event of downtime in a single long-range radar.

5.1 *1-6 km UH*

For S1, there are very small differences in the average distance and timing errors among the four different types of runs, but MYDM and MYTM have slightly larger 1-6UH ST and AT average distance errors for the NoKTLX and Neither runs (Fig. 7a,b). However, the other microphysics schemes have the largest distance errors in the Control runs. Even though there are some differences in average errors, the small, inconsistent differences in errors indicate that the forecast of 1-6UH centers, as related to S1, didn't substantially suffer from the exclusion of CASA or KTLX radar data (Fig. 7).

For S2, the NoCASA runs mostly have larger 1-6UH ST and AT average distance errors than the NoKTLX runs, but this result is not consistent among the different microphysics schemes (Fig. 8a,b). However, comparing this result to S1's results indicates that the assimilation of CASA radar data may have more of an impact on the forecast of 1-6UH centers than the assimilation of KTLX radar data when a storm is initialized within the CASA radar network.

As has been shown already, S3's average ST and AT distance errors for 2130 UTC are unequivocally worse than the other two storms, except in some cases with LIN3 and WSM6 (Fig. 9a,b). Due to the large errors, no meaningful conclusions can be drawn for S3.

5.2 *0-1 km UH*

Generally for S1, the No-KTLX and Neither runs have larger average 0-1UH ST and AT distance and timing errors than the Control and NoCASA runs (Fig. 7d,e,f). This indicates that the removal of CASA radar data from the assimilation process has a smaller impact on the low levels than the removal of KTLX radar data likely due to S1 existing outside the CASA radar network. Being that the differences between the four types of runs for only one initialization time are analyzed for this project, no meaningful results are able to be made for S2 and S3 (Figs. 8d,e,f and 9d,e,f).

6. SUMMARY AND DISCUSSION

On 24 May 2011, a tornado outbreak affected parts of central Oklahoma. For this study, three storms with violent tornadoes from this outbreak are used to evaluate the impact of assimilating CASA radar data using a microphysically-diverse set of simulations in a potential WoF setting. The evaluation of simulated MCs using the UH field compared to estimated actual tornado locations has proven to be an effective measure of model skill. The verification technique applied in the evaluation process highlights these model successes and failures and helps define expected error bounds when utilizing microphysics diversity for the WoF ensemble concept (though any operational WoF setup will have a much larger ensemble size).

Forecasting a complex real-world case yielded variations in model skill. The environment certainly was well forecasted to support several tornadic storms, but getting the details of storm rotation close-to-right is more difficult when multiple storms occur within close proximity to each other. The impact of assimilating CASA X-band radar data proved to be quite variable run-to-run and among different microphysics schemes, especially for S2 and S3. However, generally the MY schemes performed better in these experiments. Not surprisingly, the impact of assimilating CASA radar data is small for S1 due to the storm being located well to the north of the CASA radar network.

The low-levels (< 2 km AGL) of storms within the CASA radar network initially exhibit stronger horizontal and vertical circulations with the inclusion of CASA radar data (not shown), but this seemingly-important benefit has less impact on forecasts than anticipated. However, more real-time case studies like this one might need to be conducted before definitive conclusions can be drawn. For the second experiment, the NoKTLX and Neither runs need to be completed for the other seven initialization times. Perhaps these additional runs will provide clarity to the results.

As previously mentioned, the ADAS complex cloud analysis package was updated to be more compliant

with a range of cloud and precipitation microphysics schemes, and while substantial improvements were made in the initial analyses (Brewster and Stratman, 2015), additional modifications could be made for further improvements. No cycling was used in this study, but perhaps cycling or the recently-developed IAU with variable-dependent timing (Brewster et al., 2015) could be employed to potentially improve forecasts, especially for S2 and S3.

ACKNOWLEDGEMENTS

This work is supported by the National Science Foundation via CASA ERC grant EEC 03-13747 and related support provided by the University of Oklahoma (OU). Any opinions, findings, and conclusions or recommendations expressed in this material are those of the authors and do not necessarily reflect the views of the National Science Foundation. Most of the computing for this project was performed at the OU Supercomputing Center for Education & Research (OSCER). This work utilized data from the Oklahoma Mesonet provided by the Oklahoma Climatological Survey.

REFERENCES

Bloom, S. C., L. L. Takacs, A. M. da Silva, and D. Ledvina, 1996: Data Assimilation Using Incremental Analysis Updates. *Mon. Wea. Rev.*, 124, 1256–1271.

Brewster, K. A. and D. R. Stratman, 2015: An Updated High Resolution Hydrometeor Analysis System Using Radar and Other Data. *Preprints, 27th Conf. on WAF and 23rd Conf. on NWP*, Chicago, IL, 2 July 2015.

Brewster, K.A., F.H. Carr, K.W. Thomas, and D.R. Stratman, 2015: Utilizing heterogeneous radar systems in a real-time high resolution analysis and short-term forecast system in the Dallas/Ft Worth Testbed. *Preprints, 37th Conf. on Radar Meteor., Norman, OK, 18 Sept.* 2015.

Gao, J., M. Xue, K. Brewster, and K. K. Droegemeier, 2004: A three-dimensional variational data analysis method with recursive filter for Doppler radars. *J. Atmos. Oceanic Tech.*, 21, 457-469.

Hong, S.-Y., and J.-O. J. Lim, 2006: The WRF single-moment 6-class microphysics scheme (WSM6). *J. Korean Meteor. Soc.*, 42, 129–151.

Hu, M., M. Xue, and K. Brewster, 2006: 3DVAR and Cloud Analysis with WSR-88D Level-II Data for the Prediction of the Fort Worth, Texas, Tornadic Thunderstorms. Part I: Cloud Analysis and Its Impact. *Mon. Wea. Rev.*, 134, 675–698.

Hu, M., M. Xue, J. Gao, and K. Brewster, 2006: 3DVAR and Cloud Analysis with WSR-88D Level-II Data for the Prediction of the Fort Worth, Texas, Tornadic Thunderstorms. Part II: Impact of Radial Velocity Analysis via 3DVAR. *Mon. Wea. Rev.*, 134, 699–721.

Kain, J. S., S. J. Weiss, D. R. Bright, M. E. Baldwin, J. J. Levit, G. W. Carbin, C. S. Schwartz, M. L. Weisman, K. K. Droegemeier, D. B. Weber, and K. W. Thomas, 2008: Some Practical Considerations Regarding Horizontal Resolution in the First Generation of Operational Convection-Allowing NWP. *Wea. Forecasting*, 23, 931–952.

Lin, Y.-L., R. D. Farley, and H. D. Orville, 1983: Bulk Parameterization of the Snow Field in a Cloud Model. *J. Climate Appl. Meteor.*, 22, 1065–1092.

McLaughlin, D., D. Pepyne, B. Philips, J. Kurose, M. Zink, E. Knapp, D. Westbrook, E. Lyons, A. Hopf, A. DeFonzo, R. Contreras, T. Djaferis, E. Insanic, S. Frasier, V. Chandrasekar, F. Junyent, N. Bharadwaj, Y. Liu, and Y. Wang, K. Droegemeier, M. Xue, J. Brotzge, F. Carr, K. Kloesel, K. Brewster, S. Cruz-Pol, and K. Hondl, 2009: Short-Wavelength Technology and the Potential for Distributed Networks of Small Radar Systems, *Bull. Amer. Meteor. Soc.*, 90, 1797-1817.

Milbrandt, J. A. and M. K. Yau, 2005: A Multimoment Bulk Microphysics Parameterization. Part I: Analysis of the Role of the Spectral Shape Parameter. *J. Atmos. Sci.*, 62, 3051–3064.

Milbrandt, J. A. and M. K. Yau, 2005: A Multimoment Bulk Microphysics Parameterization. Part II: A Proposed Three-Moment Closure and Scheme Description. *J. Atmos. Sci.*, 62, 3065–3081.

Noilhan, J. and S. Planton, 1989: A simple parameterization of land surface processes for meteorological models. *Mon. Wea. Rev.*, 117, 536-549.

Schenkman A. D., M. Xue, A. Shapiro, K. Brewster, and J. Gao, 2011: Impact of CASA Radar and Oklahoma Mesonet Data Assimilation on the Analysis and Prediction of Tornadic Mesovortices in an MCS. *Mon. Wea. Rev.*, 139, 3422–3445.

Stensrud, D. J., L. J. Wicker, K. E. Kelleher, M. Xue, M. P. Foster, J. T. Schaefer, R. S. Schneider, S. G. Benjamin, S. S. Weygandt, J. T. Ferree, and J. P.

Tuell, 2009: Convective-Scale Warn-on-Forecast System. *Bull. Amer. Meteor. Soc.*, 90, 1487–1499.

Stensrud, D. J., L. J. Wicker, M. Xue, D. T. Dawson, N. Yussouf, D. M. Wheatley, T. E. Thompson, N. A. Snook, T. M. Smith, A. D. Schenkman, C. K. Potvin, E. R. Mansell, T. Lei, K. M. Kuhlman, Y. Jung, T. A. Jones, J. Gao, M. C. Coniglio, H. E. Brooks, K. A. Brewster, 2013: Progress and challenges with Warn-on-Forecast. *Atmos. Res.*, 123, 2-16.

Sun, W.-Y., and C.-Z. Chang, 1986: Diffusion model for a convective layer. Part I: numerical 864 simulation of convective boundary layer. *J. Climate App. Meteorol.*, 25, 1445–1453.

Trapp, R. J., and M. L. Weisman, 2003: Low-level mesovortices within squall lines and bow echoes. Part II: Their genesis and implications. *Mon. Wea. Rev.*, 131, 2804–2823.

Xue, M., K. K. Droegemeier, and V. Wong, 2000: The Advanced Regional Prediction System (ARPS) - A multiscale nonhydrostatic atmospheric simulation and prediction tool. Part I: Model dynamics and verification. *Meteor. Atmos. Physics.*, 75, 161-193.

Xue, M., K. K. Droegemeier, V. Wong, A. Shapiro, K. Brewster, F. Carr, D. Weber, Y. Liu, and D.-H. Wang, 2001: The Advanced Regional Prediction System (ARPS) - A multiscale nonhydrostatic atmospheric simulation and prediction tool. Part II: Model physics and applications. *Meteor. Atmos. Physics.*, 76, 134-165.

Xue, M., D.-H. Wang, J.-D. Gao, K. Brewster, and K. K. Droegemeier, 2003: The Advanced Regional Prediction System (ARPS), storm-scale numerical weather prediction and data assimilation. *Meteor. Atmos. Physics*, 82, 139-170.

Xue, M., J. Schleif, F. Kong, K. W. Thomas, Y. Wang, and K. Zhu, 2013: Track and Intensity Forecasting of Hurricanes: Impact of Convection-Permitting Resolution and Global Ensemble Kalman Filter Analysis on 2010 Atlantic Season Forecasts. *Wea. Forecasting*, 28, 1366–1384.

Zalesak, S. T., 1979: Fully Multidimensional Flux-Corrected Transport Algorithms for Fluids. *J. Comput. Phys.*, 31, 335–362.

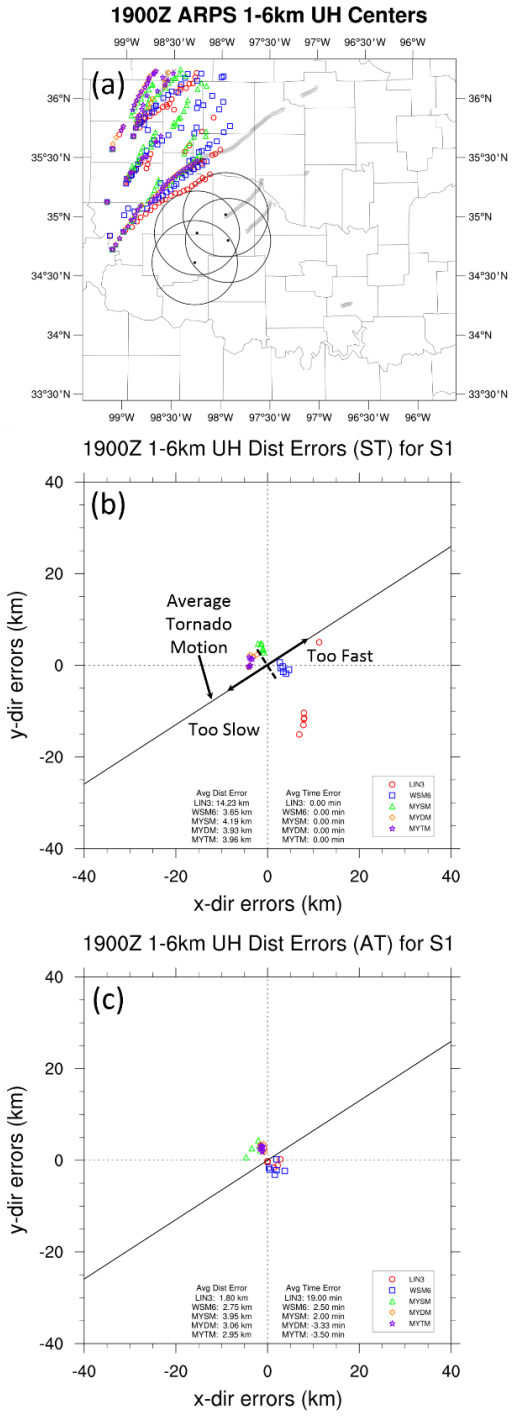

Figure 3. (a) Plot of 1–6-km UH centers from forecasts every 5 min for the 1900-UTC simulations. Small grey triangles represent estimated tornado points every 1 min, and small black triangles highlight estimated tornado points used in the ST distance error calculations for each set of simulations. Small black-filled circles represent the locations of the CASA radars, and the larger black circles indicate the 40-km range of the individual CASA radars. (b) Plot of ST 1–6-km UH centers from the 1900-UTC simulations relative to S1's estimated tornado points. See annotation in plot for additional info. (c) Same as in (b), but for AT 1–6-km UH centers.

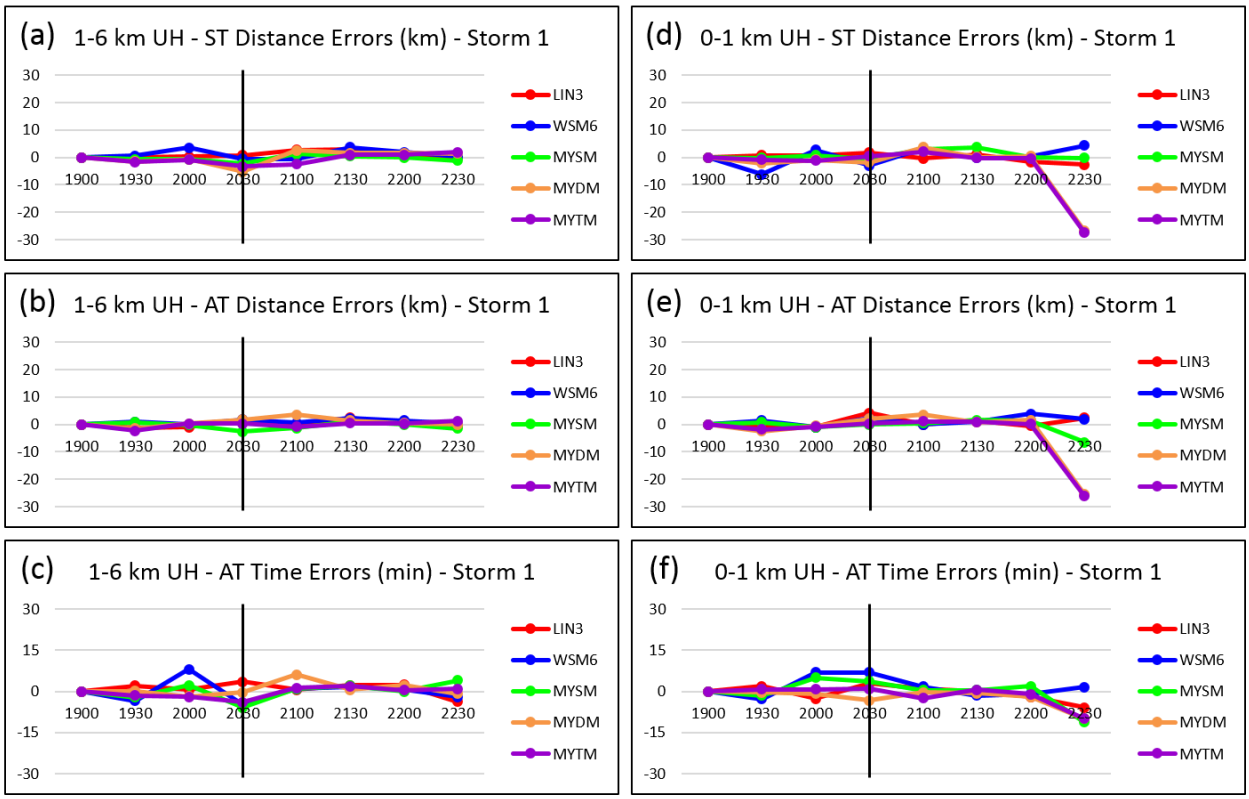

Figure 4. Differences between S1's Control and NoCASA runs for average ST distance errors (km) for (a) 1–6-km UH centers and (d) 0–1-km UH centers, average AT distance errors (km) for (b) 1–6-km UH centers and (e) 0–1-km UH centers, and absolute values of average AT time errors (min) for (c) 1–6-km UH centers and (f) 0–1-km UH centers from all simulations. Black vertical lines represent the estimated start time of S1's first tornado. Negative values indicate the Control run performed better

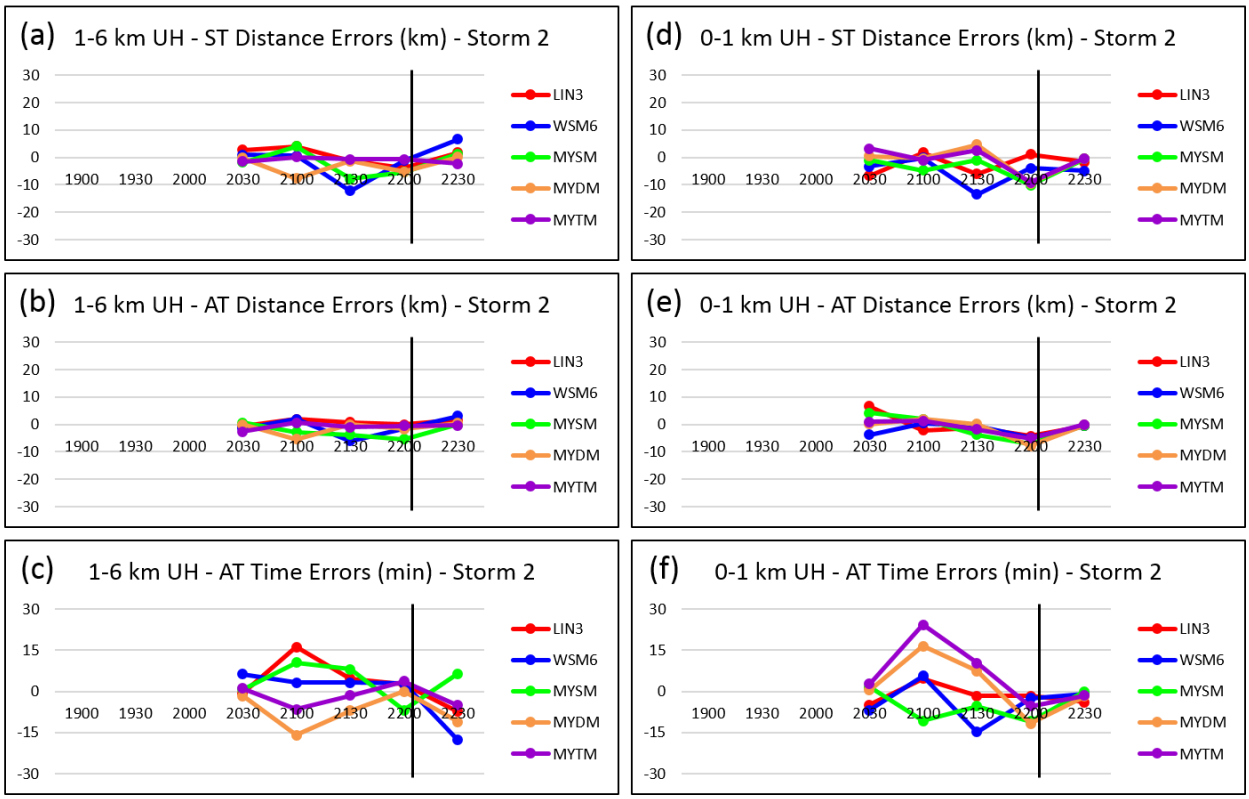

Figure 5. Same as in Fig. 4, but for S2.

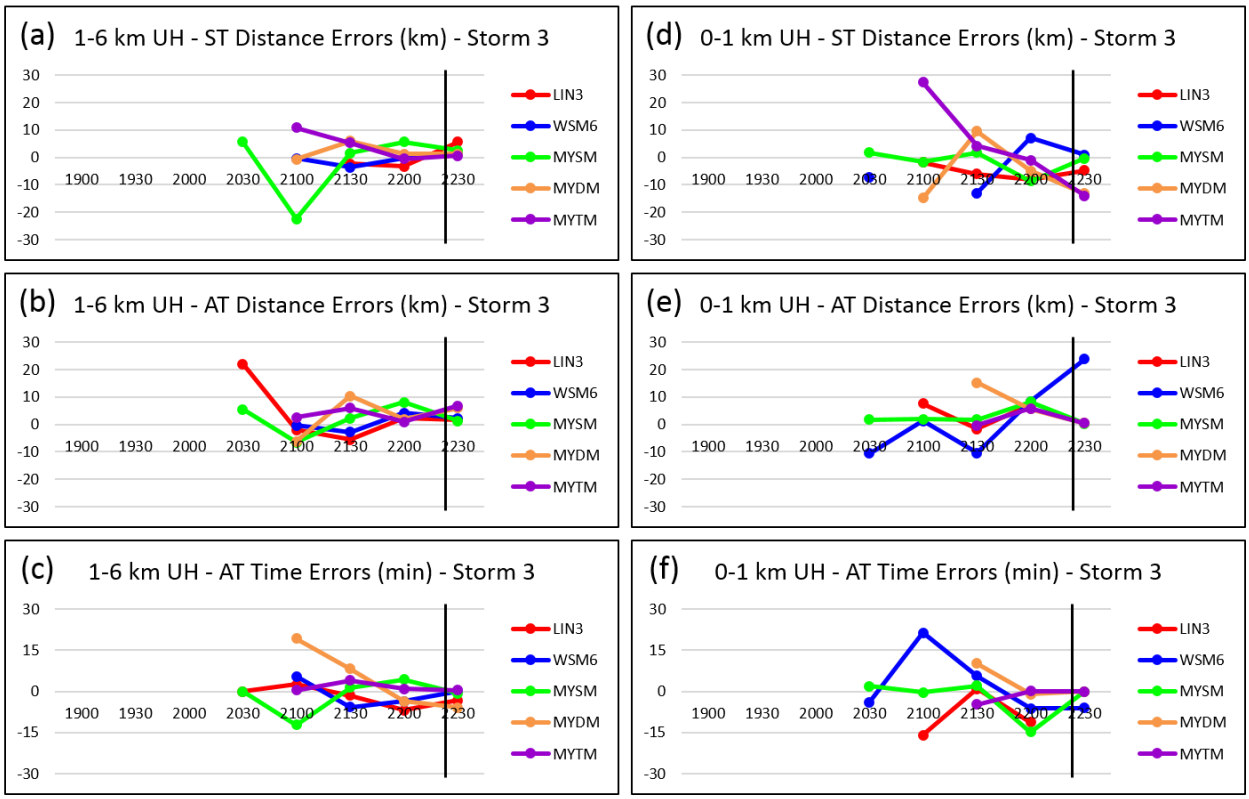

Figure 6. Same as in Fig. 4, but for S3.

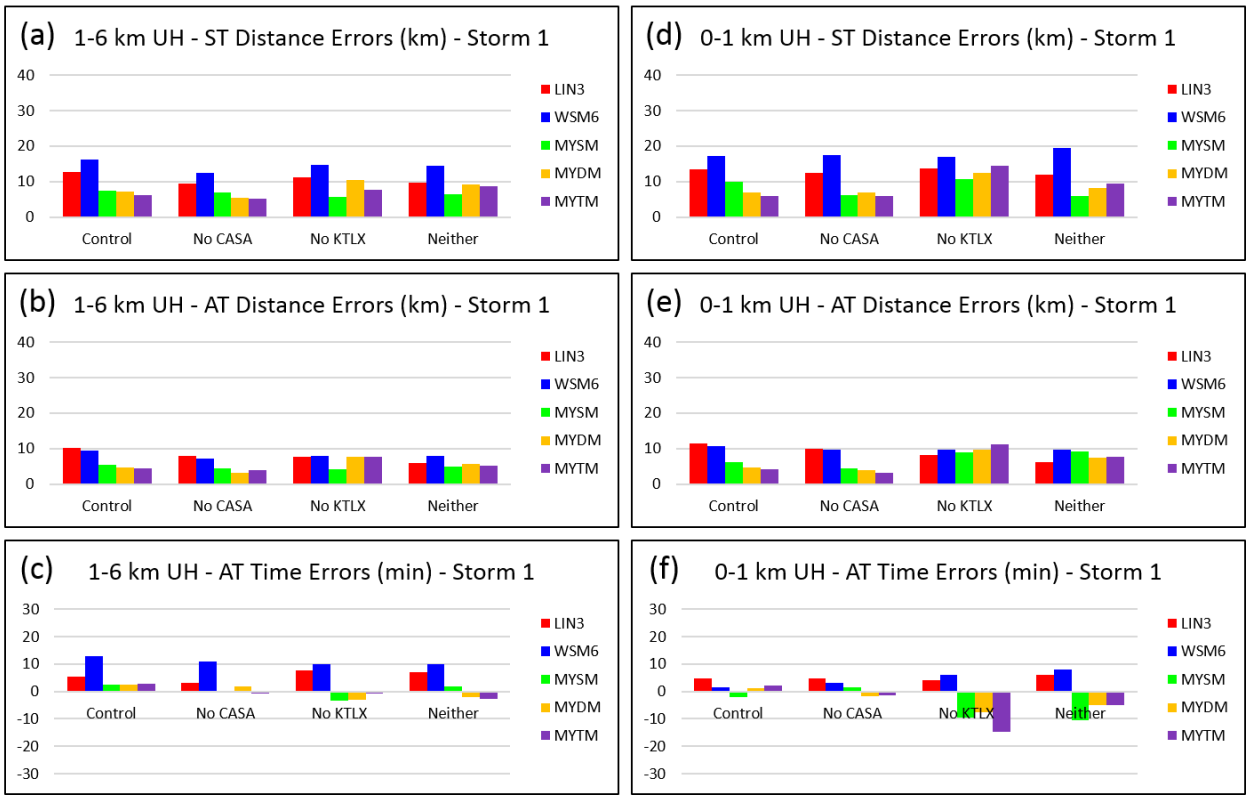

Figure 7. Column charts depicting S1's average ST distance errors for (a) 1–6-km UH centers and (d) 0–1-km UH centers, average AT distance errors (km) for (b) 1–6-km UH centers and (e) 0–1-km UH centers, and average AT time errors (min) for (c) 1–6-km UH centers and (f) 0–1-km UH centers from the 2130-UTC simulations.

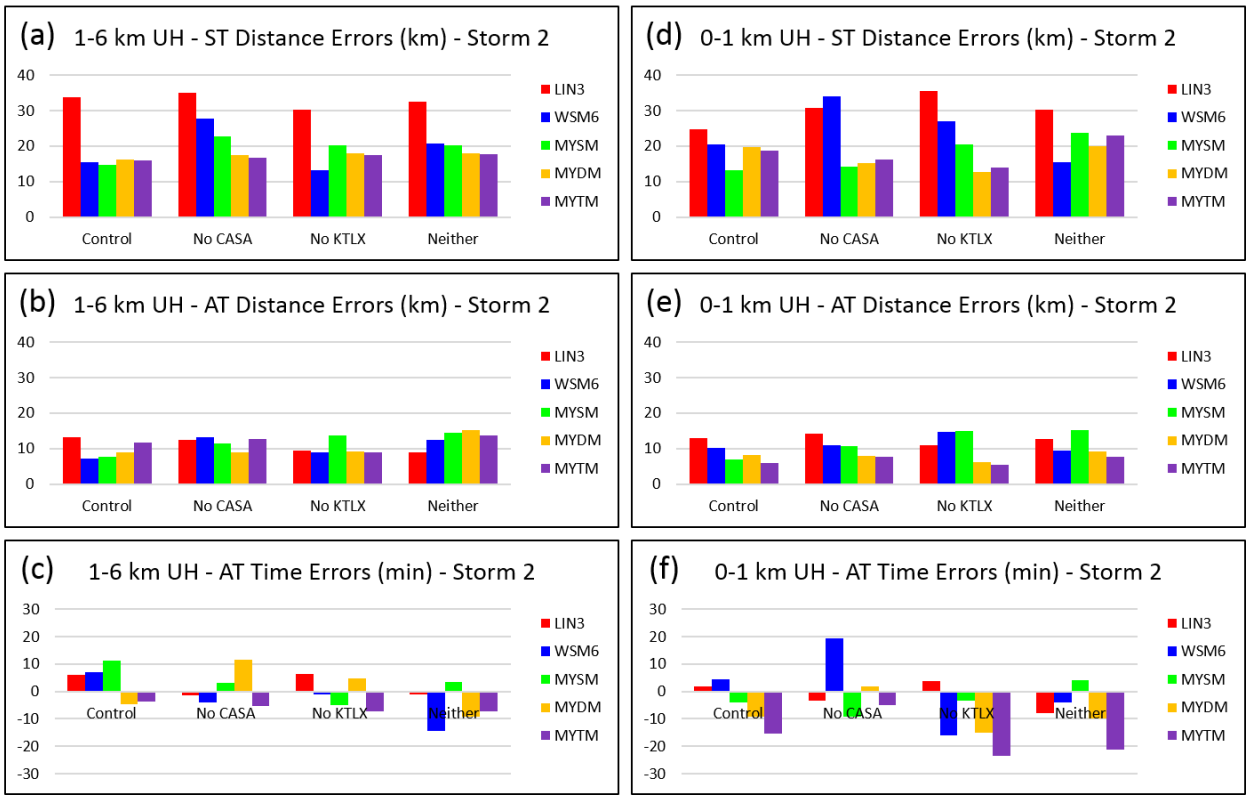

Figure 8. Same as in Fig. 7, but for S2.

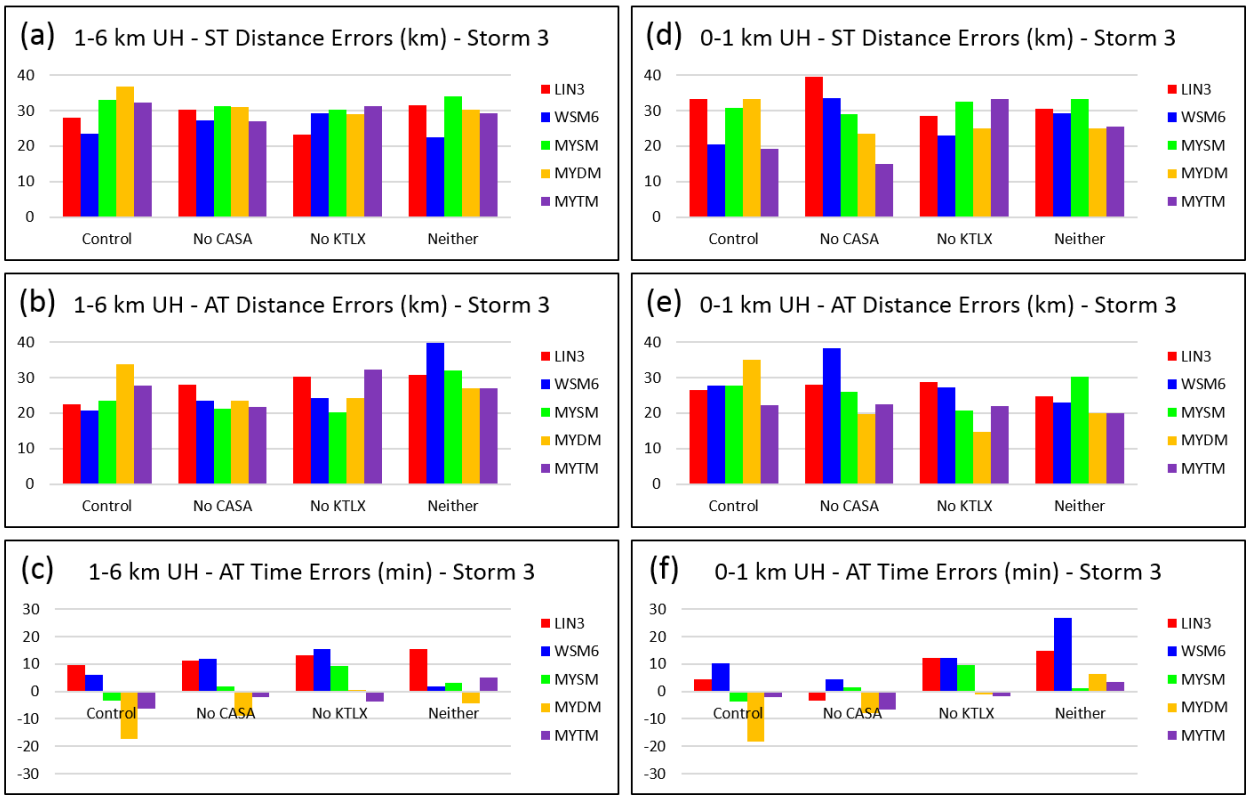

Figure 9. Same as in Fig. 7, but for S3.